Volume 1 | Number 1 | Jan 2013 | Pages 1–100

Journal of
Materials Chemistry C

Materials for optical and electronic devices
www.rsc.org/materialsC

ROYAL SOCIETY
OF CHEMISTRY

ROYAL SOCIETY
OF CHEMISTRY

www.rsc.org/materialsC

Journal Name

ARTICLE

Light driven growth of silver nanoplatelets on 2D MoS$_2$ nanosheet templates

T. Daeneke[a*], B. Carey[a], A. Chrimes[a], J. Zhen Ou[a], D.W.M. Lau[b], B.C. Gibson[b], M. Bhaskaran[c] and K. Kalantar-zadeh[a*]

A novel synthesis approach for the fabrication of silver nanoparticles and platelets using MoS$_2$ nanosheets has been investigated herein, which is based on the direct photo excitation of the semiconductor bandgap in the presence of silver ions. The silver ions were effectively reduced to silver metal and a range of silver–MoS$_2$ heterostructures were synthesised, depending on illumination time. Short light exposure led to the formation of silver nanoparticles on the MoS$_2$ sheets. Longer illumination time led to a templated growth mechanism and the formation of large silver nanoplatelets, fully encapsulating the MoS$_2$ templates. These silver nanoplatelets were found to self-assemble into large micrometre sized silver nanodendrites / nanobranches which were effectively used as a surface enhanced Raman spectroscopy platform.

Introduction

Two dimensional transition metal dichalcogenides (TMDs) such as MoS$_2$ have recently received increased attention due to their unique properties.[1] MoS$_2$ forms a hexagonal crystal structure, where the metal atoms are located in a distinct layer between two sulfur layers establishing a two dimensional MoS$_2$ sheet.[1, 2] In the naturally occurring bulk 2H MoS$_2$ many sheets are bound to each other by weak Van der Waals forces. By reducing the number of MoS$_2$ sheets and reaching the fundamental plane of unit cell thickness, distinctive properties arise, which hold promise for the development of the next generation electronic circuits, optical systems, plasmonic devices, catalysts, sensors and biomedically favorable compounds.[3-25]

Single and few layers MoS$_2$ are readily accessible and can be synthesised following one of the methods that have so far been developed.[2, 26-32] Recently nanocompounds of thin layered MoS$_2$ and noble metal nanoparticles have emerged, having shown to possess interesting optical and catalytic properties especially with regards to hydrogen evolution catalysis and photo decomposition of organic pollutants in water.[23, 33-45] These noble metal decorated MoS$_2$ sheets were most commonly synthesised by reducing their associated ions utilising sodium borohydride, hydrazine and other reducing agents, often in the presence of capping agents.[33, 34, 36, 40, 41] In this work we follow a different approach based on photodeposition to achieve the growth of silver nanoparticles, on the surface of two

dimensional (2D) MoS$_2$ nanosheets (see Scheme 1). Photoinduced growth of silver nanoparticles in absence of MoS$_2$ nanosheets is routinely achieved, resulting in the formation of a range of nanoparticle morphologies (e.g. prisms and plates). This synthesis method typically relies on the chemical synthesis of silver seed particles followed by the transformation and growth of these particles under illumination.[46]

In this work, the 2D MoS$_2$ nanosheets function as the seeding and templating base for the silver nanoparticles. In contrast to the photoinduced transformation of silver seed particles to form larger nano morphologies, this approach utilizes the bandgap of the MoS$_2$ semiconductor sheet for the photocatalytic reduction and deposition of silver on the MoS$_2$ surface. When light is absorbed by the MoS$_2$ sheet an electron hole pair is generated. If the energy offset between the redox potential of the silver salt in solution and the energy level of the conduction band of the MoS$_2$ is sufficient, charge transfer can occur leading to the reduction and deposition of silver. The positive charge (hole) is expected to engage in water oxidation when moisture is present or the oxidation of organic solvent molecules is involved.[50, 51] Deposited silver nanoparticles coalesce and grow further in time to expand into silver nanoplatelets, enveloping the MoS$_2$ nanosheet. A similar approach has been demonstrated for the growth of silver nanoparticles on TiO$_2$ surfaces.[47-49]

Utilising the photoreduction approach silver-MoS$_2$ nanocomposites (Ag@MoS$_2$) with pristine silver surfaces are produced, since no capping agent is used. This is particularly

beneficial for catalysis applications and sensing in which the exposure of the silver atoms to the target analytes is critical, while also avoiding the use of unstable and hazardous chemicals such as sodium borohydride and hydrazine.
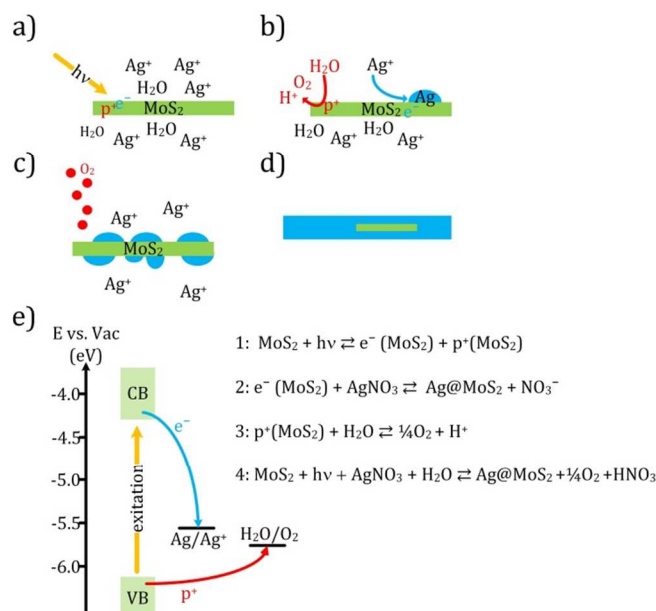
Scheme 1: a – d) Schematic illustration of the photo induced templated growth process of Ag onto 2D MoS_2 nanosheets and, **e)** energy diagram of the photoreaction and the chemical equations of the reactions involved (energy levels were taken from selected literature)[50-53]

Results and Discussion

The 2D MoS_2 nanosheets were synthesised using a grinding assisted ultrasonic exfoliation method.[54] The literature method has been modified by utilizing mechanised ball milling rather than manual grinding using mortar and pestle. Ball milling was found to be a suitable replacement for the irreproducible manual grinding step, leading to highly concentrated MoS_2 nanosheet suspensions. The pristine 2D MoS_2 nanosheets and light driven template growth of silver onto 2D MoS_2 nanosheet templates were characterised by transmission electron spectroscopy (TEM). Figure 1a shows the initial pristine MoS_2 nanosheets that have been used as the template. The lateral dimensions and flake thickness of the MoS_2 nanosheets were determined using TEM and atomic force microscopy (AFM). The typical lateral size was found to be 120±55 nm, while the flake thickness was determined to be 1.2±0.4 nm (See Figure S1 and S2 in the supplementary information (SI) for sample AFM images and size distributions) with 26% single, 58% double and 16% triple or more layer nanosheets.

Figure 1 b to f show the MoS_2 nanoheets after set time intervals of the photodeposition process. It can be clearly seen that silver nanoparticles grow rapidly on the MoS_2 surface once illuminated. The elemental map shown in Figure S3 in the supplementary information, created by analysing the energy disperse X-ray (EDX) spectrum of the sample measured using scanning transmission electron microscopy that clearly identifies silver features on 2D MoS_2 flakes.

The presence of some small silver nanoparticles at t=0 min (Figure 1 b) can be rationalised by the presence of room light illumination during the reaction mixture and potentially the rapid reaction of $AgNO_3$ with surface defects and charges present from the exfoliation process.[35] With increasing light exposure time, more silver nanostructures emerge and the sizes of all silver nanoparticles increase until they join together (Figure 1 e and f). After 90 min, large sized silver agglomerates, sometimes up to several millimeters in length, have formed which were removed by centrifugation. The amber suspension was illuminated a further 45 min to ensure the full conversion of $AgNO_3$ to metallic silver. TEM imaging revealed that upon completion of the reaction (90+45 min) large silver nanoplatelets have formed (Figure 1 g) with relatively polydisperse lateral dimensions of 420±270 nm (mean value), featuring some single platelets exceeding 1000 nm and typical thicknesses of 53±32 nm. Electron diffraction patterns and high resolution TEM images reveal that the final silver platelets are highly crystalline silver particles terminating with a (111) facet (see Figure 1 h and i). The prominent inner reflections in the selective area electron diffraction pattern correspond to a lattice spacing of 2.5 Å which can be identified as the 1/3 (422) forbidden reflection that is observed due to stacking faults of the (111) planes.[55] The TEM images of silver functionalised MoS_2 sheets illuminated for short time periods indicate a templated growth mechanism in which the silver is growing around the MoS_2 flake, fully encapsulating the template and further grow into much larger platelets in time (see Table S1 in the supplementary information for statistical analysis of the silver nanoparticle sizes for short illumination times). A control experiment was conducted in which 10 mM $AgNO_3$ dissolved in a 90% N-methyl-2-pyrrolidone (NMP) and 10% H_2O mixture were illuminated in the absence of 2D MoS_2 flakes following the same synthesis protocol. No growth was observed under this condition, confirming that the MoS_2 templates are crucial for the synthesis (data not shown).

Thick bulk particles that are comprised of many MoS_2 layers bound through van der Waals forces are also found in liquid phase exfoliated MoS_2 sheet suspension since the exfoliation yield is not quantitative. Interestingly, silver growth was exclusively observed on very thin MoS_2 flakes and small numbers of pristine bulk MoS_2 particles were observed at all stages throughout the templated growth (SI Figure S4). Bulk MoS_2 possesses a significantly lower energy bandgap compared to single layer MoS_2 (1.3 and 1.9 eV, respectively), changing the position of the valence and conduction band edges, most likely prohibiting crucial steps during the photoinduced chain reaction detailed in Scheme 1.[53] Furthermore the bandgap of bulk MoS_2 is indirect, leading to a reduced extinction coefficient and an increased charge carrier recombination rate, decreasing the probability of surface reactions to occur even further.[1, 10]
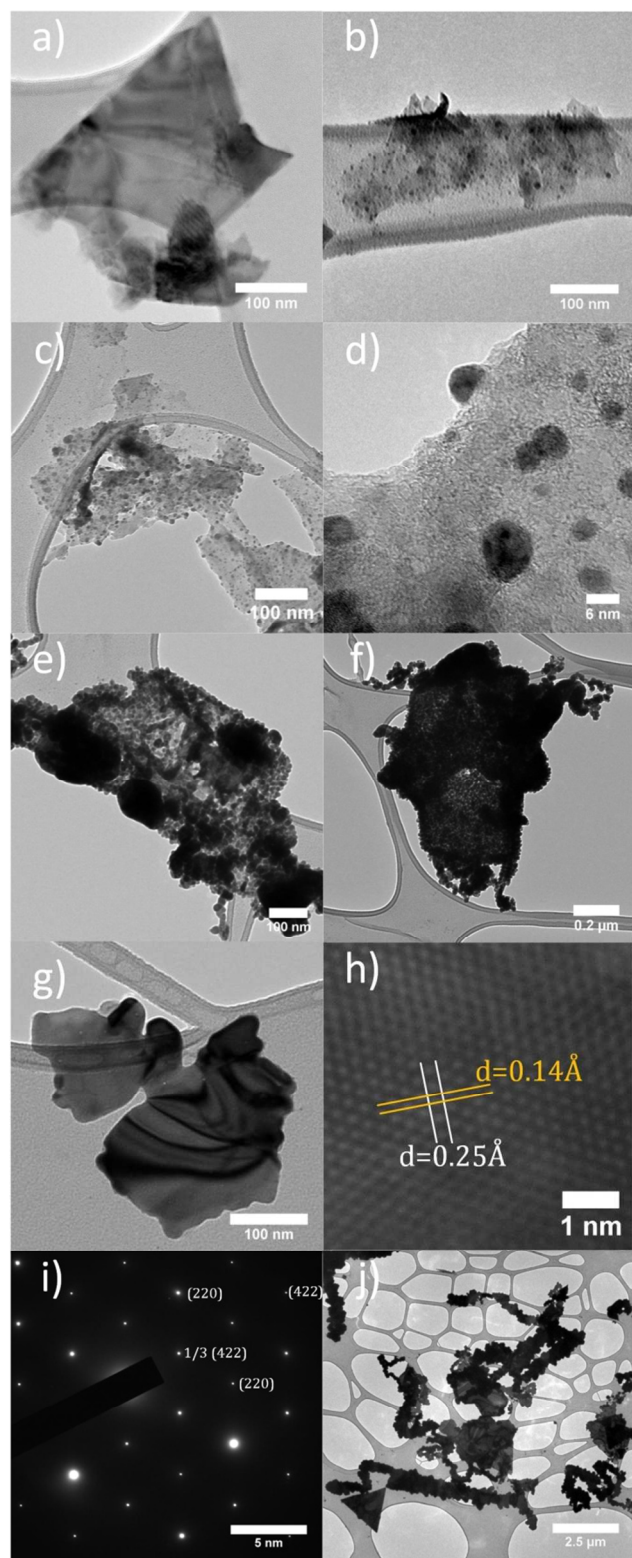
Figure 1: TEM images **a)** of the initial MoS_2 flakes that were used as template; **b)** MoS_2 flakes at t=0 min prior to the light exposition; **c)** and **d)** low magnification and high resolution TEM images after 5 min of light; **e)** and **f)** TEM images after 10 and 20 min of light exposure respectively; **g)** silver platelet after 90+45 min of light exposure; **h)** high resolution TEM image of a silver platelet; **i)** electron diffraction pattern of a silver platelet and **j)** TEM image of the self-assembled silver nanodendrites / nanobranches

In order to investigate this hypothesis further, two samples were prepared using filtered light. A 700 nm (1.77 eV) and a 825 nm (1.5 eV) filter were used, allowing to excite either all multilayer MoS_2 nanosheets or all nanosheets with 3 and more layers, since the band gap of bilayer MoS_2 is approximately 1.5 eV, 1.9 eV for single layer MoS_2 and below 1.5 eV for multi-layer nanosheets.[56] No silver growth was observed under the filtered light conditions (See Figure S5). This observation highlights the necessity of working with thin MoS_2 nanosheets for photochemical reactions for achieving successful results.

Upon prolonged storage of the silver nanoplatelets (days), a precipitate was formed. The precipitate could be easily isolated by centrifugation (4000 rpm 5 min) followed by suspension in NMP. TEM images revealed that the precipitate is the result of a self-assembly reaction of the silver nanoplatelets into several micrometer long, low order dendrimer / nanobranch like silver nanostructures with heterogeneous morphologies (Figure 1j). This self-assembly reaction occurs predominantly along the highly reactive edges of the silver platelets since the large flat (111) facets are comparatively inert, leading to the formation of silver nanodendrites / nanobranches.[57] These silver nanobranches are of great interest for the fabrication of sensors based on surface enhanced Raman spectroscopy (SERS) due to their high crystallinity and large number of edges and corners, providing strong enhancement of Raman signals.[58] Furthermore similar structures such as silver nanodendrites, nanowires and nanobelts have found applications in energy storage, catalysis and transparent conductive coatings.[58, 59] The here developed photo-induced templated growth of silver on 2D MoS_2 flakes provides ample access to a range of nanostructures ranging from silver nanoparticle decorated MoS_2 flakes to silver nanoplatelets templated onto the flakes.

To further characterise the samples photoluminescence (PL) spectra were taken for the initial templates, the final silver platelets and MoS_2 flakes which have been illuminated for 135 min (90+45 min) in absence of any silver salt (control) (see Figure 2). Intriguingly it was observed that illuminating the MoS_2 flakes in the control experiment led to an enhancement of the PL. This can be rationalised by the decomposition and removal of surface impurities through photooxidation and reduction processes, similar to the ones observed in TiO_2 photocatalysts.[60] In the case of the silver nanoplatelets, the PL spectra resembles overall the spectra of the templating MoS_2 particles, showing minor PL enhancement when excited at 375 and 400 nm and a slight blue shift of 5 to 10 nm. This highlights that the electronic properties of the final heterostructure are dominated by the MoS_2 templates. The PL of the silver nanobranches was characterised in the dry state after drop casting the suspension onto a Si wafer due to the intense scattering and fast sedimentation of the silver nanobranches in suspension. PL maps and spectra were recorded for the silver nanobranches and the MoS_2 templates (See Figure S6-9 in the SI). The PL maps resolved the characteristic shape of the silver nanobranches while the PL spectra of the nanobranches strongly resembled the spectra of the MoS_2 templates indicating that the electronic properties of

the encapsulated MoS_2 sheets have been preserved. The PL spectra of the silver nanoplatelets and the silver nanobranches together with the TEM study support the proposed templated

growth mechanism leading to the encapsulation of the template by metallic silver.
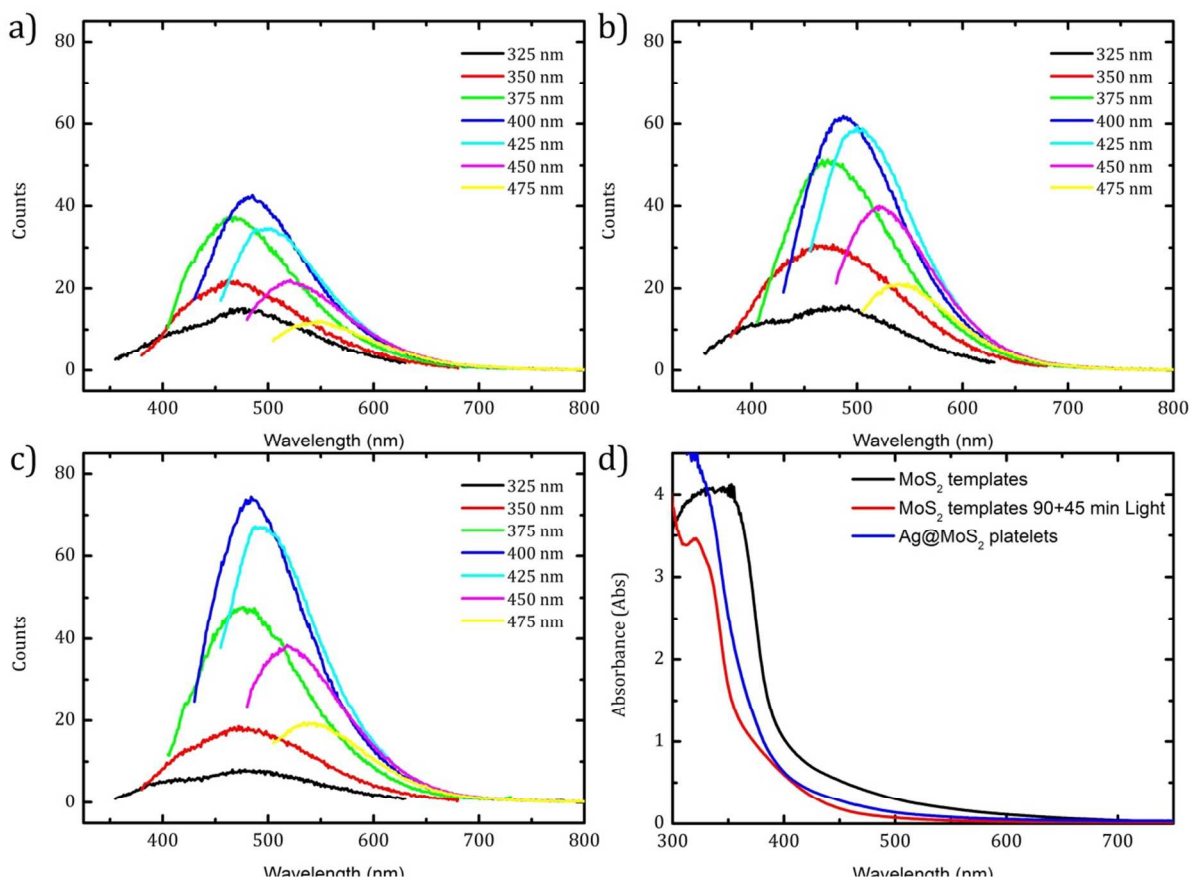

Figure 2: a) PL spectra of the MoS_2 stock solution diluted 1:25 in a NMP H_2O mixture (90:10) (equivalent concentration to the reaction mixture) after exfoliation and prior to the light exposure, excited at various wavelengths as indicated; **b)** PL spectra of the MoS_2 stock solution diluted 1:25 in a NMP H_2O mixture (90:10) after 90+45 min of illumination; **c)** PL spectra of the reaction product (silver nanoplatelets) after 90+45 min of illumination and centrifugation; **d)** UV-vis spectra of the MoS_2 templates, the MoS_2 templates after illumination and the final silver platelets

The UV-vis spectrum of the silver nanoplatelets is very similar to the UV-vis spectrum of the MoS_2 templates (see Figure 2d). The absorption spectrum of the MoS_2 sheets in absence of silver ions experiences a blue shift upon illumination for 90+45 min which is consistent with the removal of surface impurities and contaminations. Consistent with observations in the literature, the exitonic features of MoS_2 are not observed in the UV-vis spectra due to the use of NMP as a solvent and relatively small dimensions of the flakes.[61]

Investigation of surface enhanced Raman spectroscopy sensors

The large lateral dimension of the silver nanobranches combined with the thin nature of these particles, and the high crystallinity offer the opportunity to utilise them as a surface enhanced Raman spectroscopy (SERS) platform. For this experiment, the model compound 1-phenyl-5-mercaptotetrazole (PMT) (see Figure S10 in the SI for the chemical structure) was adsorbed onto the silver surface. PMT is a well-studied molecule that is known for its high affinity to metal surfaces

which led to its application as a corrosion inhibitor and antifogging agent in silver based photography.[62, 63] Adsorption was achieved by suspending the silver nanobranches in a 1 mM solution of PMT for 10 min. Due to the large size of the nanobranches the silver particles could be easily isolated by 3 steps of washing with fresh NMP followed by 5 min of centrifugation. The particles were then drop casted onto a gold coated wafer and analyzed using Raman spectroscopy and mapping. The size of the silver nanobranches makes them easily observable using optical microscopy allowing to focus on a particle and to correlate the measured Raman spectrum with a specific position on the nanobranch (see Figure 3).
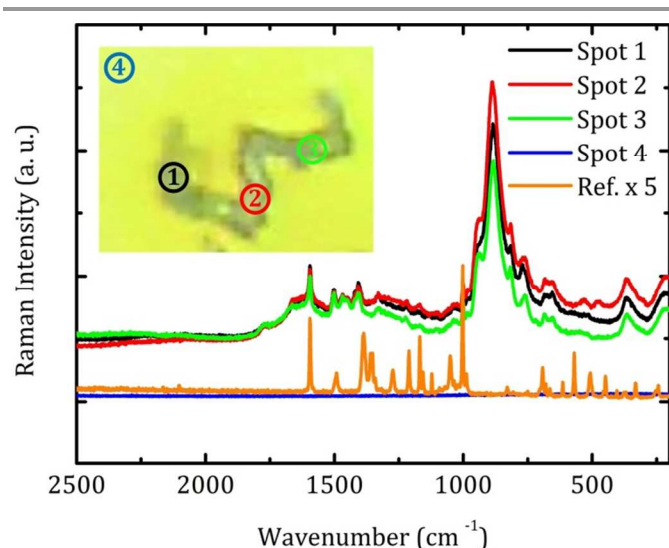
Figure 3: Raman spectra of PMT measured as powder (orange) and absorbed onto a silver nanobranch (black, red, green and blue). The Raman spectrum of the powder (reference) has been multiplied by a factor of 5. The inset shows an optical image of the silver nanobranch. The numbers in the inset indicate the location of the Raman measurements on the silver particle.

Figure 3 shows the Raman spectrum of PMT measured as a dry powder. The inset of Figure 3 shows an optical picture of the selected areas on a silver nanobranch which was investigated during the SERS studies. The numbers in the optical picture indicate the location where Raman spectra were collected. It can be seen that no Raman signal is observable for spot 4 which is located offside the silver particle on the blank gold coated wafer. Spot 1-3 are located at different areas on the nanobranch. The overall Raman spectrum for all three locations was found to be quite similar while featuring some variations in their intensity. The strongest feature is observed at 880 cm^{-1} which has been associated with torsion and vibration in the phenyl moiety of PMT.[63, 64] Similarly the feature at 1600 cm^{-1} has been associated with rotations and stretches in the phenyl group. This may be indicating that the PMT molecules adsorb in an ordered fashion on the silver surface with the phenyl group being positioned for ideal enhancement. The mode at 367 cm^{-1} has been associated with parts of the tetrazole and phenyl rings as well as the sulfur atom which is bound to the surface. The count rates increase overall by a factor of 10 when using the silver nanobranches due to the SERS effect when compared to the pure crystalline PMT powder. Raman maps were prepared for the Raman stretches at 1600, 880 and 367 cm^{-1} (see Figure 4 b c and d). The Raman spectrum was found to vary with excitation wavelength due to the excitation of other bonds (see Figure S11 and S12 in SI).

The Raman maps reveal the intense enhancement on and around the silver nanobranches. The Raman maps correspond well to the shape of the investigated particle, considering the resolution limitations of the Raman spectrometer (~500 nm). Count rates reached up to 60000 for the most intense peaks while no signal was evident from the gold substrate highlighting the suitability of the silver nanobranches as a

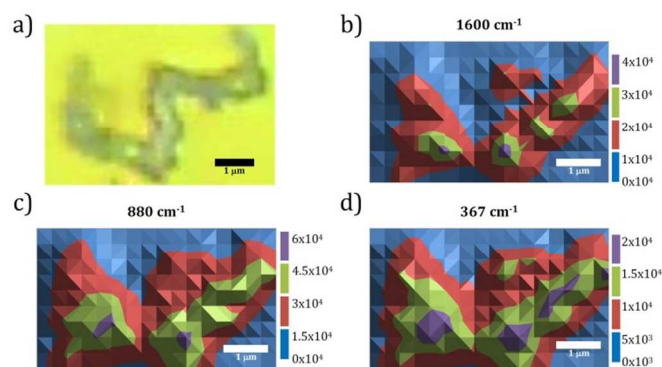SERS platform especially for SERS mapping and possibly the detection of organic materials at low concentrations.

Figure 4: a) Optical image of the investigated silver nanobranch; **b, c** and **d)** Raman maps plotted for the Raman signals measured at 1600, 880 and 367 cm^{-1}

Experimental

Synthesis of Ag decorated MoS$_2$ nanotemplates

MoS$_2$ nanosheets were prepared following a modified literature method utilising the grinding assisted ultrasonic exfoliation approach.[2, 61] Bulk MoS$_2$ particles with an average size of 2 μm (2g) were ball milled together with 20 mL of N-methyl-2-pyrrolidone (NMP) in a zirconia ball milling jar utilising zirconia grinding media (10 g of 3 to 5 mm diameter balls) in a Spex SamplePrep 8000M ball mill for 100 min. The resulting suspension was transferred into a glass jar and ultrasonicated using a Sonica Q500 probe sonicator for 90 min (100 W; 20 kHz). After sonication the slurry was centrifuged at 4000 rpm for 90 min to give a dark brown supernatant of MoS$_2$ nanosheets. The suspension was used without further purification and was found to be stable for several weeks without any signs of sedimentation or degradation.

The concentrated MoS$_2$ suspension was diluted for the photoreaction to achieve a considerable transparency (1 in 25 dilution). The final reaction mixture contained 10 mM AgNO$_3$ and 400 μL of the concentrated MoS$_2$ nanosheet stock solution. NMP and milli-Q water were added to make up a final volume of 10 mL with a solvent mixture of 90% NMP and 10% H$_2$O. The reaction mixture was vigorously stirred while illuminating with an ABET technologies 150 W Xe lamp at a distance of 10 cm (see Figure S13 in the SI for further details). At set time intervals (5, 10, 15 and 20 min) a small portion of the reaction mixture was taken to prepare TEM grids in order to elucidate the growth mechanism and characterise intermediate reaction states. The reaction mixture was irradiated for 90 min after which large quantities of metallic silver had precipitated in the form of large millimeter sized aggregates. The precipitate was removed by centrifugation at 4000 rpm for 90 min. The supernatant was illuminated for a further 45 minutes to ensure the complete conversion of AgNO$_3$ to metallic silver, followed by a further centrifugation step (4000 rpm; 90 min). The amber supernatant was then collected and characterised. The

suspension was found to be stable for several hours, after several days a gray precipitate formed. This precipitate was collected by centrifugation (5 min at 4000 rpm) and was separately characterised.

Characterization

Transmission electron microscopy (TEM) was carried out on JEOL 1010 and JEOL JEM-2100F instruments equipped with Orius CCD cameras. EDX was conducted on the JEOL JEM-2100F microscope operating in scanning transmission electron microscopy mode utilizing an Oxford XMax 80T detector. The samples were prepared by dropping 15 to 25 µl of the sample suspension onto a 300 mesh copper lacey carbon grid (ProSciTech, Australia). Lateral sizing of the analysed particles was achieved by measuring the dimensions of 100 particles utilizing the imageJ software, allowing to calculate the average lateral size and its standard deviation.

UV-Vis spectroscopy was carried out on a Varian Cary 500 spectrometer in dual beam mode using quartz cuvettes. PL spectroscopy was carried out on a Varian Cary Eclipse spectrometer utilizing quartz cuvettes and various excitation wavelengths as indicated. PL mapping was carried out on a custom build instrument using a Quantum GEM 532 nm and a Fianium WhiteLase (WL-SC400-8 - 405 nm) laser for excitation delivering 6-8 µW of laser light at the sample position. A Nikon air objective (100X 0.9NA), in combination with a 532 nm (or 405 nm) notch filter were used. For the PL mapping 25 µl of the sample were drop casted onto a silicon wafer and dried at 60°C.

Raman spectra and maps were obtained using a Renishaw micro-Raman spectrometer (InVia Streamline microscope) with a 514 nm laser source at 0.75 mW power. The resolution of the Raman maps is approximately 500 nm. A 488 and 785 nm excitation source were used for additional measurements presented in the SI. Samples for Raman spectroscopy were prepared by drop casting 100 µl of the sample solution on a gold coated (100 nm evaporated gold) silicon wafer heated at 60°C.

A D3100 Digital Instrument Atomic force microscope in tapping mode was used to measure the thickness of the flakes. Samples for AFM were prepared by drop casting 10 µl of the sample solution on a silicon wafer heated to 60°C. The height profiles were analyzed utilizing the Gwyddion software to give the average flake thickness and its standard deviation.

Conclusions

In this work, we demonstrated the photoinduced growth of silver nanoplatelets on MoS_2 templates. The reaction relies on the alignment of the redox potential of the noble metal salt in solution with the valence and conduction band edges of the MoS_2 nanosheets. It was found that silver growth occurs exclusively on thin monolayer thick MoS_2 sheets which feature a higher energy bandgap (1.9 eV) compared to multilayer (<1.5 eV) and bulk MoS_2 (1.3 eV) which failed to be functionalised

during the photoreaction. The photoreaction discussed in this manuscript is distinct from previously published methods since no harmful reducing agents were used and no capping agents were necessary. This leaves pristine surfaces of silver and allows for a comparatively easy reaction workup and short overall reaction times. A range of different nanocomposite materials was synthesised throughout the reaction which may be of interest for a host of applications. In the initial stages of the photoinduced templated growth, MoS_2 sheets are functionalised with small silver nanoparticles with diameters of 4 to 7 nm. With increasing illumination time (10 to 20 min) the size and number of silver nanoparticles increases on the MoS_2 templates. After 10 min of illumination most silver nanoparticles have joined with at least one neighbor forming a continuous silver network on the MoS_2 template. These results promise control over the final nanocomposite morphology upon further optimisation of the reaction parameters. After completion of the photoreaction, the templates are fully encapsulated with highly crystalline silver nanoplatelets sizing on average 420 nm with a typical thickness of 50 nm. These silver nanoplatelets then self-assembled into elongated silver nanodendrites/ nanobranches measuring several micrometers in length. PL and UV-vis measurements revealed that the electronic properties of the nanocomposite materials are dominated by the MoS_2 templates. SERS investigations demonstrated the viability of the silver nanobranches on a model organic material. While the nanocomposites synthesised during shorter illumination periods may find application in catalysis and sensing, it was demonstrated within this work that the silver nanobranches can be utilised as a platform for SERS measurements and SERS-mapping.

The synthesis approach developed within this work is likely to be transferable to other TMDs and different noble metals, provided that the redox potential of the noble metal salt is well aligned with the conduction and valence band edges of the chosen TMD nanosheets. This may be the focus of future investigations.

Acknowledgements

Notes and references

[a] School of Electrical and Computer Engineering, RMIT University, Melbourne, Victoria, 3001, Australia

[b] Australian Research Council Centre of Excellence for Nanoscale BioPhotonics, RMIT University, Melbourne, Victoria, 3001, Australia

[c] Functional Materials and Microsystems Research Group, School of Electrical and Computer Engineering, RMIT University, Melbourne, Victoria 3001, Australia

[*] Correspondence to Torben.Daeneke@RMIT.edu.au or Kourosh.Kalantar@RMIT.edu.au

1. Q. H. Wang, K. Kalantar-Zadeh, A. Kis, J. N. Coleman and M. S. Strano, *Nat Nanotechnol*, 2012, 7, 699-712.
2. J. N. Coleman, M. Lotya, A. O'Neill, S. D. Bergin, P. J. King, U. Khan, K. Young, A. Gaucher, S. De, R. J. Smith, I. V. Shvets, S. K. Arora, G. Stanton, H.-Y. Kim, K. Lee, G. T. Kim, G. S. Duesberg, T. Hallam, J. J. Boland, J. J. Wang, J. F. Donegan, J. C. Grunlan, G. Moriarty, A. Shmeliov, R. J. Nicholls, J. M. Perkins, E. M. Grieveson, K. Theuwissen, D. W. McComb, P. D. Nellist and V. Nicolosi, *Science*, 2011, 331, 568-571.
3. W. Wu, L. Wang, Y. Li, F. Zhang, L. Lin, S. Niu, D. Chenet, X. Zhang, Y. Hao, T. F. Heinz, J. Hone and Z. L. Wang, *Nature*, 2014, 514, 470-474.
4. Y. Wang, J. Z. Ou, A. F. Chrimes, B. J. Carey, T. Daeneke, M. M. Y. A. Alsaif, M. Mortazavi, S. Zhuiykov, N. Medhekar, M. Bhaskaran, J. R. Friend, M. S. Strano and K. Kalantar-Zadeh, *Nano Lett.*, 2015.
5. Y. Sun, S. Gao, F. Lei and Y. Xie, *Chem Soc Rev*, 2015, 623-636.
6. K. Roy, M. Padmanabhan, S. Goswami, T. P. Sai, G. Ramalingam, S. Raghavan and A. Ghosh, *Nat Nanotechnol*, 2013, 8, 826-830.
7. B. Radisavljevic, A. Radenovic, J. Brivio, V. Giacometti and A. Kis, *Nat Nanotechnol*, 2011, 6, 147-150.
8. D. Merki and X. Hu, *Energy Environ Sci*, 2011, 4, 3878-3888.
9. K. Mao, Z. Wu, Y. Chen, X. Zhou, A. Shen and J. Hu, *Talanta*, 2015, 132, 658-663.
10. K. F. Mak, C. Lee, J. Hone, J. Shan and T. F. Heinz, *Phys. Rev. Lett.*, 2010, 105, 136805.
11. K. F. Mak, K. He, J. Shan and T. F. Heinz, *Nat Nanotechnol*, 2012, 7, 494-498.
12. O. Lopez-Sanchez, D. Lembke, M. Kayci, A. Radenovic and A. Kis, *Nat Nanotechnol*, 2013, 8, 497-501.
13. X. Liu, T. Galfsky, Z. Sun, F. Xia, E.-c. Lin, Y.-H. Lee, S. Kéna-Cohen and V. M. Menon, *Nat Photonics*, 2015, 9, 30-34.
14. Q. Li, N. Zhang, Y. Yang, G. Wang and D. H. L. Ng, *Langmuir*, 2014, 30, 8965-8972.
15. D. Lembke, S. Bertolazzi and A. Kis, *Acc. Chem. Res.*, 2015, 48, 100-110.
16. J. Lee, P. Dak, Y. Lee, H. Park, W. Choi, M. A. Alam and S. Kim, *Sci. Rep.*, 2014, 4.
17. T. Jiang, H. Liu, D. Huang, S. Zhang, Y. Li, X. Gong, Y.-R. Shen, W.-T. Liu and S. Wu, *Nat Nanotechnol*, 2014, 9, 825-829.
18. X. Hong, J. Kim, S.-F. Shi, Y. Zhang, C. Jin, Y. Sun, S. Tongay, J. Wu, Y. Zhang and F. Wang, *Nat Nanotechnol*, 2014, 9, 682-686.
19. T. Heine, *Acc. Chem. Res.*, 2014, 48, 65-72.
20. M.-R. Gao, J.-X. Liang, Y.-R. Zheng, Y.-F. Xu, J. Jiang, Q. Gao, J. Li and S.-H. Yu, *Nat Commun*, 2015, 6.
21. G. Fiori, F. Bonaccorso, G. Iannaccone, T. Palacios, D. Neumaier, A. Seabaugh, S. K. Banerjee and L. Colombo, *Nat Nanotechnol*, 2014, 9, 768-779.
22. G. Du, Z. Guo, S. Wang, R. Zeng, Z. Chen and H. Liu, *Chem. Commun.*, 2010, 46, 1106-1108.
23. L. Britnell, R. M. Ribeiro, A. Eckmann, R. Jalil, B. D. Belle, A. Mishchenko, Y.-J. Kim, R. V. Gorbachev, T. Georgiou, S. V. Morozov, A. N. Grigorenko, A. K. Geim, C. Casiraghi, A. H. C. Neto and K. S. Novoselov, *Science*, 2013, 340, 1311-1314.
24. D. Akinwande, N. Petrone and J. Hone, *Nat Commun*, 2014, 5.
25. Y. Chen, C. Tan, H. Zhang and L. Wang, *Chem Soc Rev*, 2015.
26. J. T. Han, J. I. Jang, H. Kim, J. Y. Hwang, H. K. Yoo, J. S. Woo, S. Choi, H. Y. Kim, H. J. Jeong, S. Y. Jeong, K.-J. Baeg, K. Cho and G.-W. Lee, *Sci. Rep.*, 2014, 4.
27. S. Jeong, D. Yoo, M. Ahn, P. Miró, T. Heine and J. Cheon, *Nat Commun*, 2015, 6.
28. Q. Ji, Y. Zhang, Y. Zhang and Z. Liu, *Chem Soc Rev*, 2015.
29. R. Lv, J. A. Robinson, R. E. Schaak, D. Sun, Y. Sun, T. E. Mallouk and M. Terrones, *Acc. Chem. Res.*, 2014, 48, 56-64.
30. M. Naguib and Y. Gogotsi, *Acc. Chem. Res.*, 2014, 48, 128-135.
31. Y. Shi, H. Li and L.-J. Li, *Chem Soc Rev*, 2015.
32. J. Zheng, H. Zhang, S. Dong, Y. Liu, C. Tai Nai, H. Suk Shin, H. Young Jeong, B. Liu and K. Ping Loh, *Nat Commun*, 2014, 5.
33. X. Huang, Z. Zeng, S. Bao, M. Wang, X. Qi, Z. Fan and H. Zhang, *Nat Commun*, 2013, 4, 1444.
34. R. Patakfalvi, D. Diaz, P. Santiago-Jacinto, G. Rodriguez-Gattorno and R. Sato-Berru, *J Phys Chem C*, 2007, 111, 5331-5336.
35. Y. Shi, J.-K. Huang, L. Jin, Y.-T. Hsu, S. F. Yu, L.-J. Li and H. Y. Yang, *Sci. Rep.*, 2013, 3.
36. T. S. Sreeprasad, P. Nguyen, N. Kim and V. Berry, *Nano Lett.*, 2013, 13, 4434-4441.
37. H. Sun, J. Chao, X. Zuo, S. Su, X. Liu, L. Yuwen, C. Fan and L. Wang, *RSC Adv*, 2014, 4, 27625-27629.
38. C. Tan and H. Zhang, *Chem Soc Rev*, 2015.
39. X. Xia, Z. Zheng, Y. Zhang, X. Zhao and C. Wang, *Sens Actuators B Chem*, 2014, 192, 42-50.
40. L. Zhou, B. He, Y. Yang and Y. He, *RSC Adv*, 2014, 4, 32570-32578.
41. J. Zhao, Z. Zhang, S. Yang, H. Zheng and Y. Li, *J Alloys Compd*, 2013, 559, 87-91.
42. L. Pan, Y.-T. Liu, X.-M. Xie and X.-D. Zhu, *Chem Asian J*, 2014, 9, 1519-1524.
43. S. Su, C. Zhang, L. Yuwen, J. Chao, X. Zuo, X. Liu, C. Song, C. Fan and L. Wang, *ACS Appl Mater Interfaces*, 2014, 6, 18735-18741.
44. B. G. Rao, H. Matte and C. N. R. Rao, *J. Cluster Sci.*, 2012, 23, 929-937.
45. L. Yuwen, F. Xu, B. Xue, Z. Luo, Q. Zhang, B. Bao, S. Su, L. Weng, W. Huang and L. Wang, *Nanoscale*, 2014, 6, 5762-5769.
46. G. P. Lee, Y. Shi, E. Lavoie, T. Daeneke, P. Reineck, U. B. Cappel, D. M. Huang and U. Bach, *ACS Nano*, 2013, 7, 5911-5921.
47. L. P. Wen, B. S. Liu, C. Liu and X. J. Zhao, *J Wuhan Univ Technol*, 2009, 24, 258-263.
48. P. D. Cozzoli, R. Comparelli, E. Fanizza, M. L. Curri, A. Agostiano and D. Laub, *J. Am. Chem. Soc.*, 2004, 126, 3868-3879.
49. S. C. Chan and M. A. Barteau, *Langmuir*, 2005, 21, 5588-5595.
50. H. L. Zhuang and R. G. Hennig, *Chem Mater*, 2013, 25, 3232-3238.
51. Y. Liu, Y.-X. Yu and W.-D. Zhang, *J Phys Chem C*, 2013, 117, 12949-12957.
52. N. G. Connelly and W. E. Geiger, *Chem. Rev.*, 1996, 96, 877-910.
53. J. Low, S. Cao, J. Yu and S. Wageh, *Chem. Commun.*, 2014, 50, 10768-10777.
54. N. G. Shang, P. Papakonstantinou, S. Sharma, G. Lubarsky, M. Li, D. W. McNeill, A. J. Quinn, W. Zhou and R. Blackley, *Chem. Commun.*, 2012, 48, 1877-1879.
55. V. Germain, J. Li, D. Ingert, Z. L. Wang and M. P. Pileni, *J Phys Chem B*, 2003, 107, 8717-8720.
56. N. Scheuschner, O. Ochedowski, A.-M. Kaulitz, R. Gillen, M. Schleberger and J. Maultzsch, *Phys. Rev. B*, 2014, 89, 125406.
57. P. Yu, J. Huang and J. Tang, *Nanoscale Res Lett*, 2011, 6, 46.
58. L. Wang, H. Li, J. Tian and X. Sun, *ACS Appl Mater Interfaces*, 2010, 2, 2987-2991.
59. N. Wang, X. Cao, Q. Chen and G. Lin, *Chem. Eur. J.*, 2012, 18, 6049-6054.
60. C. S. Turchi and D. F. Ollis, *J Catal*, 1990, 122, 178-192.
61. E. P. Nguyen, B. J. Carey, T. Daeneke, J. Z. Ou, K. Latham, S. Zhuiykov and K. Kalantar-zadeh, *Chem Mater*, 2014, 27, 53-59.
62. X. R. Ye, X. Q. Xin, J. J. Zhu and Z. L. Xue, *Appl Surf Sci*, 1998, 135, 307-317.
63. B. Pergolese and A. Bigotto, *J Raman Spectrosc*, 2002, 33, 646-651.
64. B. Pergolese and A. Bigotto, *J Mol Struct*, 2003, 655, 479-489.

Journal of Materials Chemistry C Accepted Manuscript

TOC figure and text
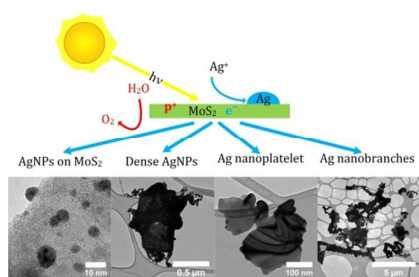
This work investigates a novel synthesis strategy for the functionalisation of 2D MoS_2 nanosheets with silver. Direct excitation of the MoS_2 bandgap was found to lead to the photodeposition and eventual planar growth of metallic silver on the 2D MoS_2 nanosheet templates.